NUMERICAL SIMULATION OF FLUID-STRUCTURE INTERACTION REPRESENTED BY HUMAN VOCAL FOLD

J. Valášek [1], P. Sváček [1]

[1] **Department of Technical Mathematics, Faculty of Mechanical Engineering, Czech Technical University in Prague, Karlovo nám. 13, Praha 2, 121 35, Czech Republic**

Abstract

This paper deals with derivation of mathematical model and implementation of fluid-structure interaction. It is coupled problem. Firstly the whole problem is described by partial differential equations including boundary conditions on common interface. ALE method is used to capture time variable shape of fluid domain. Secondly numerical model is derived. Finite element method is utilized for discretization in space for structure and fluid part of problem. The BDF2 scheme was implemented for time discretization of fluid flow and the Newmark method was applied for time solution of elastic body deformation. In the end numerical results are presented.

Keywords: finite element method, 2D Navier-Stokes equations, vocal folds, aeroelasticity

1 Introduction

The flow driven vibration of elastic bodies is a problem investigated and solved in many technical applications. This paper deals with biomechanics of human vocal folds, see e.g. [14]. Human voice is one of basic human being's characteristics and it plays an important role in the quality of a human life. The air flow from lungs excites the vibrations of the human folds which setting is influenced by the human muscles and causes the human voice production. Therefore the attention is further devoted for better understanding of this complex process. This problem was studied in many papers, for example see [9], [13]. Nevertheless, the main goal of this paper is to develop a simplified model for fluid-structure interaction (FSI) and to verify it's basic functionality.

Here, we focus on the derivation of mathematical model and on the development of on it based numerical algorithm. This implemented algorithm we verify on a few test cases, where only low Reynolds number was involved. For the analysis of results were Fourier transformation and modal analysis utilized. The numerical method is based on finite element method (FEM). For the fluid solver the cross-grid P1 elements and for the elastic part P1 elements are implemented. The Arbitrary Lagrangian-Eulerian (ALE) method is involved for handling with the time-dependent domain. For the coupled problem the full-implicit scheme is used.

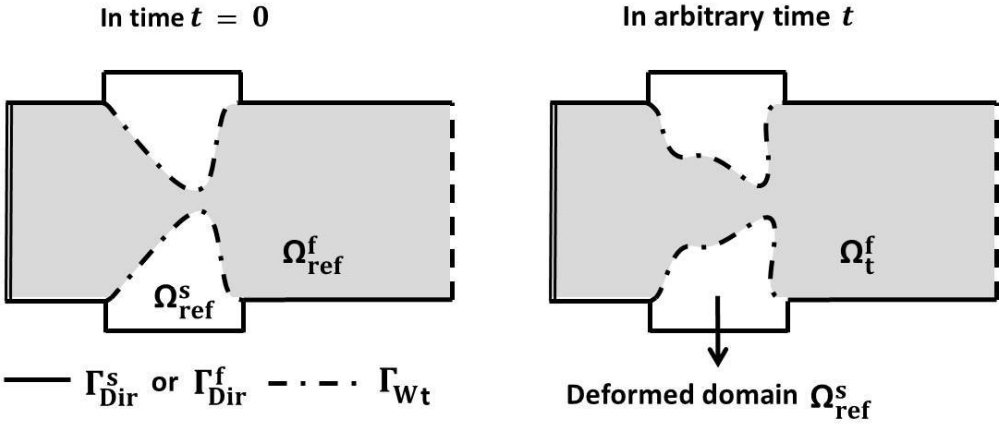

Figure 1: Schema of vocal folds model with boundaries marked before and after deformation.

2 Mathematical model

The vocal fold model is considered as 2D model in this paper. A scheme of the problem model is shown in Figure 1, where Ω^s_{ref} denotes the reference representation of the structure, Ω^f_{ref} is the domain occupied by the fluid at the time instant $t = 0$ (also reference) and $\Gamma_{\mathrm{W_{ref}}} = \Gamma_{\mathrm{W_0}}$ is the common interface. At instant time t structure domain is deformated to shape Ω^s, but it is treated in reference (Lagrangian) coordinates and therefore $\Omega^s = \Omega^s_{ref}$. On the other hand the fluid domain is considered in generalized Eulerian-Lagrangian coordinates so Ω^f_{ref} turns to Ω^f_t in time t and ALE method has to be used.

ALE method. Arbitrary Lagrangian-Eulerian method (ALE) is generalization of Eulerian and Lagrangian description of investigated domain. It is assumed there exists diffeomorphism A_t, which maps reference domain Ω^f_{ref} to computational domain Ω^f_t in any time $t \in [0, \mathrm{T}]$. This mapping satisfies

$$A_t : \overline{\Omega}^f_{ref} \longrightarrow \overline{\Omega}^f_t, \text{ t.j. } X \in \overline{\Omega}^f_{ref} \longmapsto x = \tilde{x}(X,t) = A_t(X) \in \overline{\Omega}^f_t, \tag{1}$$

where X denotes point in domain $\overline{\Omega}^f_{ref}$ and x denotes point in domain $\overline{\Omega}^f_t$. In addition we suppose to A_t fulfill

$$\frac{\partial A_t}{\partial t} \in C(\overline{\Omega}^f_{ref}), \quad A_t(\partial\Omega_{ref}) = \partial\Omega^f_t, \quad t \in [0, \mathrm{T}]. \tag{2}$$

Then we name this mapping A_t ALE mapping.

It should be mention that A_t does not trace real motion of the fluid as it is posed in Lagrangian coordinates. A_t just maps Ω^f_{ref} to time dependent domain Ω^f_t. The differences between Eulerian, Lagrangian and ALE coordinates are shown in Figure 2.

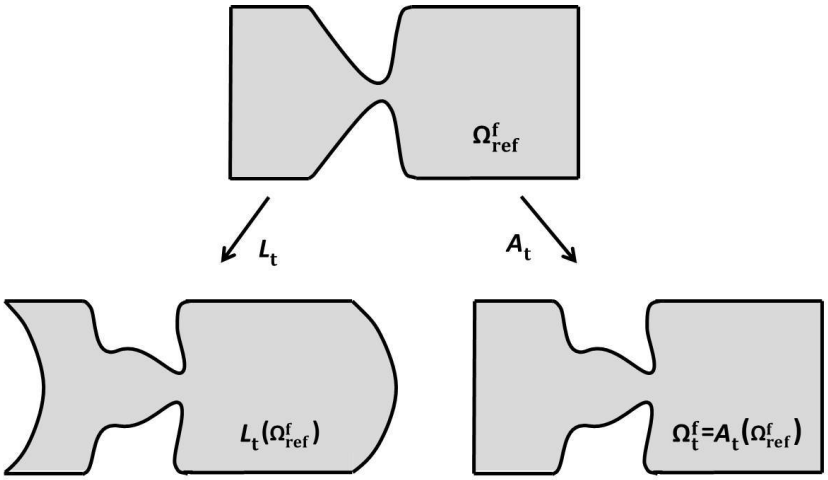

Figure 2: Differences between Eulerian, Lagrangian description (represented by L_t) and ALE mapping A_t.

Now we can define the velocity of the domain deformation $\mathbf{w}_D$ as

$$\mathbf{w}_D(x,t) = \hat{\mathbf{w}}_D(A_t^{-1}(x), t), \quad t \in (0, \mathrm{T}), \ x \in \Omega^f_t, \tag{3}$$

where $\hat{\mathbf{w}}_D$ is quantity defined on Ω^f_{ref} and

$$\hat{\mathbf{w}}_D(X,t) = \frac{\partial}{\partial t} A_t(X), \quad t \in (0, \mathrm{T}), \ X \in \Omega^f_{ref}. \tag{4}$$

The we can introduce so called ALE derivative of function $f = f(x,t)$ for $x \in \Omega^f_t$ and $t \in (0, \mathrm{T})$ as derivative with respect to $X \in \Omega^f_{ref}$ as

$$\frac{D^A}{Dt} f(x,t) = \frac{\partial \hat{f}}{\partial t}(X,t), \tag{5}$$

where $x = A_t(X)$ and $\hat{f}(X,t) = f(A_t(X),t)$. We apply the rule of multivariable composite function derivative which leads to

$$\frac{D^A}{Dt} f(x,t) = \frac{\partial f}{\partial t}(A_t(x),t) = \frac{\partial f}{\partial t}(x,t) + \mathbf{w}_D(x,t) \cdot \nabla f(x,t), \tag{6}$$

where $\mathbf{w}_D(x,t)$ is defined by relation (3). Further information can be found for example in [10].

Flow model. First we describe incompressible viscous fluid flow in Eulerian coordinates with partial differential equations. Fluid flow description follows from principle of mass and momentum conservation. It can be derived that the principle of mass conservation is given in differential form by

$$\frac{\partial \rho^f}{\partial t} + \text{div } (\rho^f \mathbf{v}) = 0 \quad \text{in } \Omega_t^f, \tag{7}$$

where ρ^f denotes density of fluid and $\mathbf{v}$ is fluid velocity. But we suppose incompressibility of the fluid and therefore constant fluid density so then equation (7) gets final simplified version after disivion by ρ^f

$$\text{div } \mathbf{v} = 0 \quad \text{in } \Omega_t^f. \tag{8}$$

Similarly the principle of momentum conservation must hold for each component of velocity vector. Then the equation of momentum conservation can be derived with the help of Reynold's transport theorem in the form, see [5]

$$\frac{\partial \rho^f v_i}{\partial t} + \text{div } (\rho^f v_i \mathbf{v}) = \rho^f g_i^f + \text{div } \frac{\partial \sigma_{ij}^f}{\partial x_j} \quad \text{in } \Omega_t^f, \tag{9}$$

where g_i^f is a volume force and σ_{ij}^f denotes stress tensor of fluid. After expressing tensor $\boldsymbol{\sigma}^f = -p\mathbb{I} + 2\mu^f \mathbb{D}(\mathbf{v})$, division equation (9) by constant density ρ^f, introducing kinematic pressure as $\tilde{p} = \frac{p}{\rho^f}$ and kinematic viscosity as $\nu^f = \frac{\mu^f}{\rho^f}$, we get so called Navier-Stokes equation in the vector form

$$\frac{\partial \mathbf{v}}{\partial t} + (\mathbf{v} \cdot \nabla)\mathbf{v} - \nu^f \Delta \mathbf{v} + \nabla \tilde{p} = \mathbf{g}^f. \tag{10}$$

In next we will omit writing tilde above kinematic pressure $\tilde{p}$.

Now we can reformulate derived equations (8) and (10) from Eulerian coordinates to the ALE description. The equation of continuity does not change. But in Navier-Stokes equation classical time derivative turns to ALE derivative according to (6)

$$\frac{\partial \mathbf{v}}{\partial t} = \frac{D^A \mathbf{v}}{Dt} - \mathbf{w}_D \cdot \nabla \mathbf{v}. \tag{11}$$

Then we can rewrite equation (11) to the final shape, see for example [6]

$$\frac{D^A \mathbf{v}}{Dt} + ((\mathbf{v} - \mathbf{w}_D) \cdot \nabla)\mathbf{v} - \nu^f \Delta \mathbf{v} + \nabla p = \mathbf{g}^f. \tag{12}$$

To correct formulation of the problem we must add initial and boundary conditions. We prescribe different types of boundary conditions on the different parts of boundary. The scheme of fluid domain Ω_t^f at arbitrary time t is shown in Figure 3.

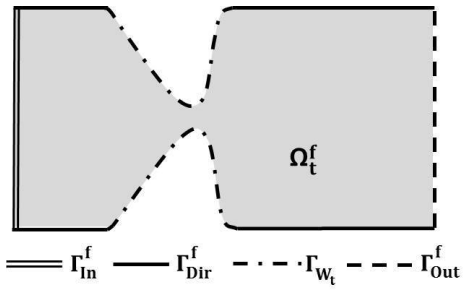

Figure 3: The computational domain Ω_t^f at the time instant t and it's boundaries.

The $\Gamma^f_{\rm In}$ is the inlet part of the boundary, $\Gamma^f_{\rm Out}$ is the outlet part of the boundary, $\Gamma^f_{\rm Dir}$ represents solid wall of the glottal channel surface and the only time dependent boundary $\Gamma_{\rm W_t}$ represents the interface on the vibrating vocal folds.

So the boundary and inital conditions are given as

$$\begin{aligned}
&\text{a)} && \mathbf{v}(x,t) = \mathbf{0} && \text{for } x \in \Gamma^f_{\rm Dir},\ t \in (0,{\rm T}),\\
&\text{b)} && \mathbf{v}(x,t) = \mathbf{v}_{\rm Dir}(x,t) && \text{for } x \in \Gamma^f_{\rm In},\ t \in (0,{\rm T}),\\
&\text{c)} && (p(x,t)-p_{ref})\vec{n} - \nu^f \frac{\partial \mathbf{v}}{\partial \vec{n}}(x,t) = \mathbf{0}, && \text{for } x \in \Gamma^f_{\rm Out},\ t \in (0,{\rm T}),\\
&\text{d)} && \mathbf{v}(x,t) = \mathbf{w}_D(x,t) && \text{for } x \in \Gamma_{\rm W_t}.\\
&\text{e)} && \mathbf{v}(x,0) = \mathbf{v}_0(x) && \text{for } x \in \Omega^f_{ref}.
\end{aligned} \tag{13}$$

Elastic structure. The vocal fold model is considered as the 2D compliant structure. The deformation $\mathbf{u}$ of the structure is given by the equations of motion

$$\rho^s \frac{\partial^2 \mathbf{u}}{\partial t^2} - \frac{\partial \tau^s_{ij}(\mathbf{u})}{\partial x_j} = \mathbf{f}^s \quad \text{in } \Omega^s \times (0,{\rm T}), \tag{14}$$

where ρ^s is the structure density, the tensor τ^s_{ij} is the Cauchy stress tensor and the vector $\mathbf{f}^s$ is the volume density of an acting force. Using the generalized Hook's law, the Cauchy stress tensor τ^s_{ij} is given by, see for example [2],

$$\tau^s_{ij} = C_{ijkl}\ e^s_{kl}, \tag{15}$$

where C_{ijkl} denotes the fourth order tensor of elastic coefficients and e^s_{jk} is the strain tensor. The strain tensor e^s_{jk} is given under assumption of small displacements by

$$e^s_{jk} = \frac{1}{2}\left(\frac{\partial u_j}{\partial x_k} + \frac{\partial u_k}{\partial x_j}\right). \tag{16}$$

In addition we assume the isotropic body. Then equation (15) can be written in the form

$$\tau^s_{ij} = \lambda^s {\rm div}\ \mathbf{u} + 2\mu^s e^s_{ij}, \tag{17}$$

where λ^s, μ^s are Lame coefficients dependent on the Young modulus of elasticity E^s and the Poisson's ratio σ^s as

$$\lambda^s = \frac{E^s \sigma^s}{(1+\sigma^s)(1-2\sigma^s)}, \quad \mu^s = \frac{E^s}{2(1+\sigma^s)}.$$

Equation (14) is supplied with the following initial and the boundary conditions

$$\begin{aligned}
&\text{a)} && \mathbf{u}(x,0) = \mathbf{u}_0(x) && \text{for } x \in\ \Omega^s,\\
&\text{b)} && \frac{\partial \mathbf{u}}{\partial t}(x,0) = \mathbf{u}_1(x) && \text{for } x \in\ \Omega^s,\\
&\text{c)} && \mathbf{u}(x,t) = \mathbf{u}_{\rm Dir}(x,t) && \text{for } x \in \Gamma^s_{\rm Dir},\ t \in (0,{\rm T}),\\
&\text{d)} && \tau^s_{ij}(x,t)\, n^s_j(x) = q^s_i(x,t), && \text{for } x \in \Gamma^s_{\rm W_t},\ t \in (0,{\rm T}),
\end{aligned} \tag{18}$$

where the boundaries $\Gamma_{\rm W_t}, \Gamma^s_{\rm Dir}$ are shown in Figure 1.

Coupling conditions. The location of the interface $\Gamma_{\rm W_t}$ varies in time and it depends on establishing force equilibrium between aerodynamic and elastic forces. On the other hand these acting forces are dependent on the position and velocity of this interface. Therefore we speak about a coupled problem.

The shape of the interface $\Gamma_{\rm W_t}$ in time t is given by the deformation $\mathbf{u}$, so

$$\Gamma_{\rm W_t} = \left\{ x \in \mathbb{R}^2 |\, x = X + \mathbf{u}(X,t),\ X \in \Gamma_{\rm W_{ref}} \right\}. \tag{19}$$

Deformation $\mathbf{u}$ is influenced by aerodynamic forces which work on structure interface via pressure and shear forces. The equilibrium is then given by the equation

$$\sum_{j=1}^{2} \tau_{ij}^{s}(X)\, n_j^s(X) = \sum_{j=1}^{2} \sigma_{ij}^{f}(x)\, n_j^s(x), \quad i = 1, 2, \quad x \in \Gamma_{\mathrm{W_t}},\ X \in \Gamma_{\mathrm{W_{ref}}}, \tag{20}$$

where σ_{ij}^f is stress tensor of fluid, $n_j^s(X)$ denotes the components of the outer normal of the structure domain to the interface $\Gamma_{\mathrm{W_{t=0}}}$ and x is computed from the known deformation $\mathbf{u}$ as $x = X + \mathbf{u}(X, t)$. The equation (20) can be rewritten as the Neumann boundary condition (18 d)

$$q_i^s(X, t) = \sum_{j=1}^{2} \sigma_{ij}^{f}(x)\, n_j^s(x), \quad i = 1, 2, \quad x \in \Gamma_{\mathrm{W_t}}, t \in (0, \mathrm{T}). \tag{21}$$

The boundary condition for fluid on the interface $\Gamma_{\mathrm{W_t}}$ is prescribed to be in correspondence with motion of the elastic body, e.g. as it was done in equation (13 d).

3 Numerical approximation

For discretization in space of the presented mathematical model represented by the partial differential equations (8), (12) and (14) was used the finite element method. The derived model is discretized in time by the Newmark and the BDF2, respectively. The time interval $[0, \mathrm{T}]$ is divided into the equidistant partition with a constant time steps Δt.

Elastic structure. The weak formulation of equation (14) must be derived to FEM can be applied. The solution $\mathbf{u}$ is sought in the space $\mathbf{V} = V \times V$, where $V = \{f \in W^{1,2}(\Omega^s) | f = 0 \text{ on } \Gamma^s_{\mathrm{Dir}}\}$, and $W^{k,p}(\Omega)$ denotes the Sobolev's space. Equation (14) is reformulated with the use of Hook's law (15) and the symmetry of stress tensor in the weak sense in space as

$$\int_{\Omega^s} \rho^s \frac{\partial^2 \mathbf{u}}{\partial t^2} \mathbf{\Phi}\ \mathrm{d}x + \int_{\Omega^s} C_{ijkl} e_{kl}^s(\mathbf{u}) e_{ij}^s(\mathbf{\Phi})\ \mathrm{d}x = \int_{\Omega^s} \mathbf{f}^s \cdot \mathbf{\Phi}\ \mathrm{d}x + \int_{\Gamma^s_{\mathrm{Neu}}} \mathbf{q}^s \cdot \mathbf{\Phi}\ \mathrm{d}S. \tag{22}$$

Futhermore, the space $\mathbf{V}$ is approximated by the finite dimensional space $\mathbf{V}_h \subset \mathbf{V}$ with the dimension $2N_h$. Thus the discrete solution can be written as a linear combination of basis functions $\mathbf{\Phi}_j \in \mathbf{V}_h$, i.e. $\mathbf{u}_h(x, t) = \sum_{j=1}^{2N_h} \alpha_j(t) \mathbf{\Phi}_j(x)$. Using this expression and labeling $\boldsymbol{\alpha} = (\alpha_i)$ the equation (3) has now the form

$$\mathbb{M}\ddot{\boldsymbol{\alpha}} + \mathbb{K}\boldsymbol{\alpha} = \mathbf{b}(t), \tag{23}$$

where the elements of the matrices $\mathbb{M} = (b_{ij}), \mathbb{K} = (k_{ij})$ and $\mathbf{b}(t) = (b_i)(t)$ are given by

$$m_{ij} = \int_{\Omega^s} \rho^s \mathbf{\Phi}_j \cdot \mathbf{\Phi}_i\ \mathrm{d}x, \quad k_{ij} = \int_{\Omega^s} C_{klmn} e_{mn}^s(\mathbf{\Phi}_j) e_{kl}^s(\mathbf{\Phi}_i)\ \mathrm{d}x, \quad b_i = \int_{\Omega^s} \mathbf{f}^s \cdot \mathbf{\Phi}_i\ \mathrm{d}x + \int_{\Gamma^s_{\mathrm{Neu}}} \mathbf{q}^s \cdot \mathbf{\Phi}_i\ \mathrm{d}S. \tag{24}$$

In practical application the damping proportional to $\mathbb{C}\dot{\boldsymbol{\alpha}}$ is often considered, where matrix $\mathbb{C}$ can be chosen as $\mathbb{C} = c_1\mathbb{M} + c_2\mathbb{K}$ with small parameters c_1, c_2. Then equation (23) changes to

$$\mathbb{M}\ddot{\boldsymbol{\alpha}} + \mathbb{C}\dot{\boldsymbol{\alpha}} + \mathbb{K}\boldsymbol{\alpha} = \mathbf{b}(t). \tag{25}$$

In the practical computation the Lagrange finite elements of the first order are used, which give the first order of accuracy in space.

Newmark's method. The Newmark's method is used for the time discretization and for the solution of ordinary differential equations of the second order in a prototype form

$$y''(t) = f(t, y(t), y'(t)) \quad \text{for } t \in (0, \mathrm{T}), \quad y(0) = y_0, \quad y'(0) = y_0'. \tag{26}$$

It's application leads to the numerical scheme

$$y_{n+1} = y_n + \Delta t y'_n + \Delta t^2 \left(\beta f_{n+1} + (\frac{1}{2} - \beta) f_n \right) \tag{27}$$

$$y'_{n+1} = y'_n + \Delta t \left(\gamma f_{n+1} + (1-\gamma) f_n \right), \tag{28}$$

where $f_n = f(t_n, y_n, y'_n), f_{n+1} = f(t_{n+1}, y_{n+1}, y'_{n+1})$. The scheme is of second order accuracy in time for the parameter choice $\beta = \frac{1}{4}, \gamma = \frac{1}{2}$, see for example [3].

Step order of solution problem (25) in new time level t_{n+1} is then simple:

Firstly we solve linear equation system acquired from (25) by substituting the value of y_{n+1}, y_{n+1} by (27) and by replacing $f_{n+1} = \boldsymbol{y}''_{n+1}$

$$\underbrace{\left(\mathbb{M} + \frac{\Delta t}{2} \mathbb{C} + \beta (\Delta t)^2 \mathbb{K} \right)}_{=\mathbb{A}} \boldsymbol{y}''_{n+1} = \boldsymbol{g}^s_{n+1}, \tag{29}$$

where $\mathbb{A}$ is iterative matrix and we denote as right side the expression $\mathbf{g}_{n+1} = \mathbf{b}_{n+1} - \mathbb{C}\mathbf{y}'_n - \frac{\Delta t}{2}\mathbb{C}\mathbf{y}''_n - \mathbb{K}\mathbf{y}_n - \Delta t \mathbb{K}\mathbf{y}'_n - \frac{1-2\beta}{2}(\Delta t)^2 \mathbb{K}\mathbf{y}''_n$. System of equations (29) is easy to be solved for example by conjugate gradient method, because the matrix $\mathbb{A}$ is composed of positive defined matrices $\mathbb{K}, \mathbb{C}, \mathbb{M}$.

Secondly we compute new values of $\boldsymbol{y}'_{n+1}$ and $\boldsymbol{y}_{n+1}$ from equations (27), where we substitute again f_{n+1} by already known value of $\boldsymbol{y}''_{n+1}$.

ALE method. The ALE mapping is treated using the elastic solver analogy because ALE method in fact maps Ω^f_{ref} to deformed Ω^f_t. This solver just solves stationary elasticity problem without any source term in given time t_n, where it is prescribed Dirichlet boundary condition as boundary condition – this condition equals deformation of common interface on $\Gamma_{\mathrm{W}_{\mathrm{t}_{\mathrm{n+1}}}}$, and otherwise equals zero.

Interesting part of this procedure is the choice of elastic parameters λ^{ALE}, μ^{ALE}. They are set specifically for each triangle of triangulation proportional to the triangle area. This choice ensures to deform small triangles along common interface $\Gamma_{\mathrm{W_t}}$ less then bigger ones inside domain Ω^f_t. This choice is based on article [8]. This arrangement helps to spread deformation on the bigger part of domain Ω^f_t and to support the stability of whole algorithm. For more details see for example [15].

Flow model. For the flow model we reverse the step order. At first we discretize equation (12) in time and then both in space. For time discretization backward differentiation formula of second order (BDF2) was used. This method is suitable for ordinary differential equations of first order, see [1]. So the ALE derivative is approximated as

$$\frac{D^A \mathbf{v}}{Dt}(x_{n+1}, t_{n+1}) \approx \frac{3\mathbf{v}^{n+1}(x_{n+1}) - 4\mathbf{v}^n(x_n) + \mathbf{v}^{n-1}(x_{n-1})}{2\Delta t}. \tag{30}$$

We denote $\overline{\mathbf{v}}^i(x_{n+1}) = \mathbf{v}^i(x_i)$, where $x_i = A_{t_i}(A^{-1}_{t_{n+1}}(x_{n+1}))$ for $i = n-1, n$. Then the scheme leads together with equation (8) to

$$\frac{3\mathbf{v}^{n+1} - 4\overline{\mathbf{v}}^n + \overline{\mathbf{v}}^{n-1}}{2\Delta t} + ((\mathbf{v}^{n+1} - \mathbf{w}^{n+1}_D) \cdot \boldsymbol{\nabla})\mathbf{v}^{n+1} - \nu^f \Delta \mathbf{v}^{n+1} + \boldsymbol{\nabla} p^{n+1} = \mathbf{g}^{f,n+1}, \tag{31}$$

$$\boldsymbol{\nabla} \cdot \mathbf{v}^{n+1} = 0.$$

Then we continue with the weak formulation. The velocity solution $\mathbf{v}$ in time t_{n+1} is sought in the functional space $\mathbf{X} = \mathbf{W}^{1,2}(\Omega^f_{t_{n+1}})$ and $q \in M = L^2(\Omega^f_{t_{n+1}})$. Further, the space of the test function is defined by

$$X = \{ f \in W^{1,2}(\Omega^f_{t_{n+1}}) | \, f = 0 \text{ on } \Gamma^f_{\mathrm{Dir}} \cup \Gamma^f_{\mathrm{In}} \cup \Gamma^f_{\mathrm{W}_{\mathrm{t}_{\mathrm{n+1}}}} \} \subset W^{1,2}(\Omega^f_{t_{n+1}}).$$

For better arrangement we will write $\mathbf{v}^{n+1}$ as $\mathbf{v}$ and $\Omega^f := \Omega^f_{t_{n+1}}$. The weak formulation in space is acquired by multiplication of the first equation (31) by $\boldsymbol{\Phi} \in \mathbf{X}$, integration over the whole domain

Ω^f and by using the Green's theorem, that results in the following equations

$$\left(\frac{3\mathbf{v}-4\overline{\mathbf{v}}^n+\overline{\mathbf{v}}^{n-1}}{2\Delta t},\boldsymbol{\varphi}\right)_{\Omega^f}+((\mathbf{v}-\mathbf{w}_D)\cdot\nabla)\mathbf{v},\boldsymbol{\varphi})_{\Omega^f}+\nu^f(\nabla\mathbf{v},\nabla\boldsymbol{\varphi})_{\Omega^f}-(p,\operatorname{div}\boldsymbol{\varphi})_{\Omega^f}=$$
$$=(\mathbf{g}^f,\boldsymbol{\varphi})_{\Omega^f}-(p_{ref},\boldsymbol{\varphi}\cdot\vec{n})_{L^2(\Gamma^f_{\mathrm{Out}})}, \qquad (32)$$
$$(q,\operatorname{div}\mathbf{v})_{\Omega^f}=0,$$

where $(\cdot,\cdot)_\Omega$ stays for the scalar product of $L^2(\Omega^f)$ or $[L^2(\Omega^f)]^2$ spaces.

The FEM then approximates spaces $\mathbf{X}$ and M by the finite dimension spaces $\mathbf{X}_h$ and M_h, so the solution $\mathbf{v}\approx\mathbf{v}_h$ can be expressed as

$$\mathbf{v}_h(x)=\sum_{j=1}^{2N_h^{vel}}\beta_j\,\boldsymbol{\varphi}_j(x),\qquad p_h(x)=\sum_{j=2N_h^{vel}+1}^{2N_h^{vel}+N_h^p}\gamma_j\,q_j(x). \qquad (33)$$

Now by using relations (33) in equations (32), which has to hold for every pair of test functions $(\boldsymbol{\varphi}_j,q_j)\in\mathbf{X}_h\times M_h$, we get the system

$$\begin{pmatrix}\mathbb{A}(\mathbf{v}_h^*) & \mathbb{B}\\ \mathbb{B}^T & 0\end{pmatrix}\begin{pmatrix}\boldsymbol{\beta}\\ \boldsymbol{\gamma}\end{pmatrix}=\begin{pmatrix}\mathbf{g}\\ \mathbf{0}\end{pmatrix}, \qquad (34)$$

where $\mathbb{A}(\mathbf{v}_h)=\frac{1}{\Delta t}\mathbb{M}+\mathbb{C}(\mathbf{v}_h^*)+\mathbb{D}$. The elements of the matrices $\mathbb{M}=(m_{ij}),\mathbb{C}=(c_{ij}),\mathbb{D}=(d_{ij})$ and components of vector $\mathbf{g}=(g_i)$ are given by

$$m_{ij}=\frac{3}{2}(\boldsymbol{\varphi}_j,\boldsymbol{\varphi}_i)_{\Omega^f},\qquad c_{ij}=((\mathbf{v}_h^*-\mathbf{w}_D)\cdot\nabla)\boldsymbol{\varphi}_j,\boldsymbol{\varphi}_i)_{\Omega^f},\qquad d_{ij}=\nu^f(\nabla\boldsymbol{\varphi}_j,\nabla\boldsymbol{\varphi}_i)_{\Omega^f}, \qquad (35)$$
$$b_{ij}=(-q_j,\operatorname{div}\boldsymbol{\varphi}_i)_{\Omega^f},\quad g_i=(\mathbf{g}^f,\boldsymbol{\varphi}_i)_{\Omega^f}-(p_{ref},\boldsymbol{\varphi}_i\cdot\vec{n})_{L^2(\Gamma^f_{\mathrm{Out}})}+\left(\frac{4\overline{\mathbf{u}}^n-\overline{\mathbf{u}}^{n-1}}{2\Delta t},\boldsymbol{\varphi}_i\right)_{\Omega^f}.$$

The system of equations (34) is non-linear. For its solution the Oseen linearization $\mathbf{v}_h^*=\mathbf{v}^n$ is used. For the solution of the system (34) the mathematical library UMFPACK is employed, see [4].

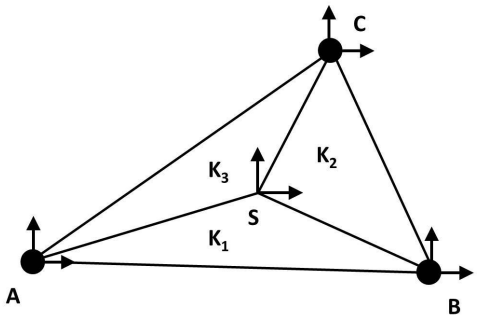

Figure 4: The crossgrid finite element for incompressible problem (P1-crossgrid/P1). Dots at vertices represent pressure variables and arrows are components of velocity.

One of the aspect of the FEM is that the choice of spaces $\mathbf{X}_h, M_h$ cannot be made randomly, but they must satisfy the well-known Babuška-Brezzi condition, see [7]. In this article P1-crossgrid/P1 elements (see Figure 4) are used, which according to [11] satisfy BB condition.

Coupled problem. Last part of our algorithm is coupling both solvers via aerodynamic forces. They are evaluated from known the velocity and pressure values at adjacent triangles to interface $\Gamma_{\mathrm{W_t}}$ according to (21)

$$q_i^s(X,t)=\sigma_{ij}^f(x)\,n_j^s(x)=\left(-p+2\nu^f\frac{1}{2}\left(\frac{\partial\mathbf{v}_i}{\partial x_j}+\frac{\partial\mathbf{v}_j}{\partial x_i}\right)\right)\,n_j^s, \qquad (36)$$

where $\mathbf{n}^s = (n_1^s, n_2^s)$ is the outer normal to boundary of the structure $\Gamma_{\mathrm{W_t}}$. The values of aerodynamic forces are computed in vertices on the interface with the help of numerical quadrature and these values are provided to elastic solver as discrete version of Neumann boundary condition.

The algorithm solving coupled problem is implemented in full-implicit form:
We start with the initial values $\mathbf{v}^0, p^0, \mathbf{u}_0, \mathbf{q}_0^s, A_{t_0}$ and $\Omega_{t_0}^f$ and $l = 0$. The index l denotes inner iteration on relevant time level. Then for $n = 0, 1, \ldots$ we proceed in computation in the following steps:

1. Based on the presented scheme (29) it is acquired new deformation $\mathbf{u}_{n+1,l}$ on n+1-th time layer and in l-th inner iteration, where $\mathbf{q}_{n+1,l}^s$ is extrapolated from $\mathbf{q}_{n+1,l-1}^s$ or $\mathbf{q}_n^s$ if $l = 0$.

2. From the known deformation $\mathbf{u}_{n+1,l}$ the ALE mapping $A_{t_{n+1,l}}$ is constructed and $\Omega_{t_{n+1,l}}^f$ is determined. Afterwards we set $\mathbf{w}_D^{n+1,l}(x) \approx \frac{3A_{t_{n+1,l}}(X) - 4A_{t_n}(X) + A_{t_{n-1}}(X)}{2\Delta t}$, where $x = A_{t_{n+1,l}}(X)$.

3. We solve (35) and we get $\mathbf{v}^{n+1,l}, p^{n+1,l}$ defined on $\Omega_{t_{n+1,l}}^f$.

4. The action of the aerodynamic forces $\mathbf{q}_{n+1,l}^s$ on the interface are determined from (36) at time t_{n+1} in l-th inner iteration from the known values $\mathbf{v}^{n+1,l}, p^{n+1,l}$.

5. We check if condition $|\mathbf{q}_{n+1,l}^s - \mathbf{q}_{n+1,l-1}^s| < \epsilon$ or if $l = 0$ condition $|\mathbf{q}_{n+1,l}^s - \mathbf{q}_n^s| < \epsilon$ holds, where ϵ is an appropriate constant.

   - If **yes**, we denote all quantities $f^{n+1} := f^{n+1,l}$, then we set $n := n + 1, l := 0$ and we continue with step 1 on the new time level.
   - If **no**, we increase $l := l + 1$ and we continue with step 1.

4 Numerical results

The numerical results for fluid flow interacting with the vocal fold model M5 suggested by paper [12] are presented. The model M5 together with the triangulation is shown in Figure 5. Here, only one half of the channel was used as the computational domain with symmetric boundary condition prescribed at the top of the fluid domain ($y = 0.003\,\mathrm{m}$).

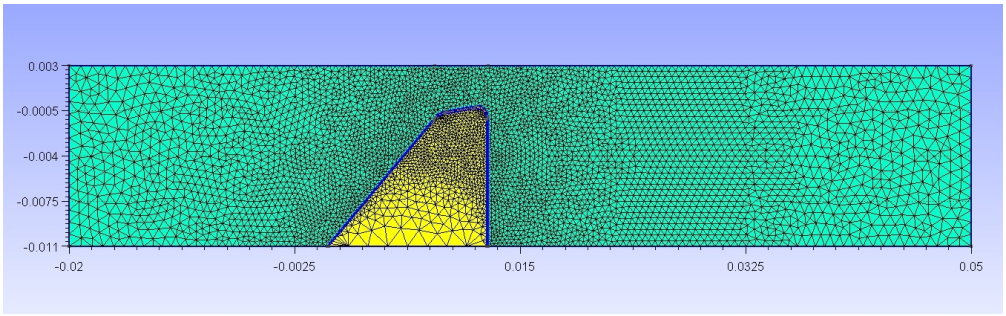

Figure 5: The triangulation of the computational domain Ω_0^f and of the vocal fold model M5 (dimensions in [m]).

Modal analysis. The eigenfrequencies of the vocal fold model were determined by modal analysis. The solution of the system of ordinary differential equations $\mathbb{M}\ddot{\mathbf{u}} + \mathbb{K}\mathbf{u} = \mathbf{0}$, where the matrices $\mathbb{M}$ and $\mathbb{K}$ are given by (24), is sought in the form $\mathbf{u} = e^{i\,\omega_j t}\mathbf{u}_j$, which leads to a generalized eigenvalue problem

$$(\mathbb{K} - \omega_j^2\,\mathbb{M})\mathbf{u}_j = \mathbf{0} \implies \det(\mathbb{K} - \omega_j^2\,\mathbb{M}) = 0. \tag{37}$$

The results are shown in Table 1 left, where the Young's modulus of elasticity was $E^s = 12$ kPa, $\sigma^s = 0,4$ inside Ω_{ref}^s and $E^s = 100$ kPa, $\sigma^s = 0,4$ in a thin layer along the interface $\Gamma_{\mathrm{W_{ref}}}$.

Frequency	[Hz]
f_1	51.43
f_2	106.34
f_3	117.36
f_4	189.76
f_5	225.11

Frequency	x-direction	y-direction
f_1	51	106
f_2	106	117
f_3	117	261

Table 1: Left: The lowest eigenfrequencies obtained from the modal analysis of model M5. Right: The significant eigenfrequencies obtained from the spectral analysis of the time signal at the point A in structure test.

Dynamics of elastic structure, energy conservation test. Furthermore, the solution of the system (23) with zero body forces and non-zero initial conditions but without fluid interaction was approximated by FEM, and the time signal of a chosen point A $[x = 0.0113\,\mathrm{m}, y = -0.0032\,\mathrm{m}]$ was analyzed by Fourier transformation. The initial conditions were $\mathbf{u}_1 = \mathbf{0}$ and

$$\mathbf{u}_0(x,y) = \begin{pmatrix} 0 \\ 0.005 \times (y + 0.011) \end{pmatrix}.$$

The obtained frequencies for the motion of the point A are shown in Table 1 right. The frequencies agree well with the modal analysis results summarized in Table 1 left.

Another possibility, how to verify solver of elastic body, is to control energy conservation of vibrating structure. The total energy E^s consists of sum of kinetic and potential energy – $E^s = E^s_{kin} + E^s_{pot}$. These energies E^s_{kin}, E^s_{pot} are given and then approximated in discrete form as

$$E^s_{kin} = \frac{1}{2}\int_{\Omega^s} \rho^s \dot{\mathbf{u}}^2 \,\mathrm{d}x \approx \frac{1}{2}\dot{\mathbf{u}}^T \mathbb{M}\dot{\mathbf{u}}, \qquad E^s_{pot} = \frac{1}{2}\int_{\Omega^s} C_{ijkl} e_{ij}(\mathbf{u}) e_{kl}(\mathbf{u}) \,\mathrm{d}x \approx \frac{1}{2}\mathbf{u}^T \mathbb{K}\mathbf{u}. \tag{38}$$

The results shown in Figure 6 confirm energy conservation of implemented procedure (no damping was considered). For comparison the same test case was simulated with damping constants $c_1 = c_2 = 5\times10^{-5}$. Results of this case are shown in Figure 7 and it is obvious that energy is considerably decreasing.

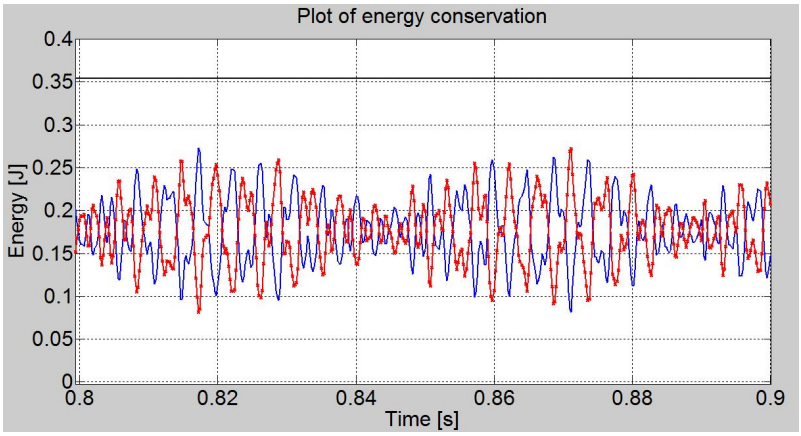

Figure 6: Graph of energy conservation, potential energy E^s_{pot} is plotted with red colour and crosses, kinetic energy E^s_{kin} is pictured by blue colour and behaviour of total energy E^s is shown with black colour.

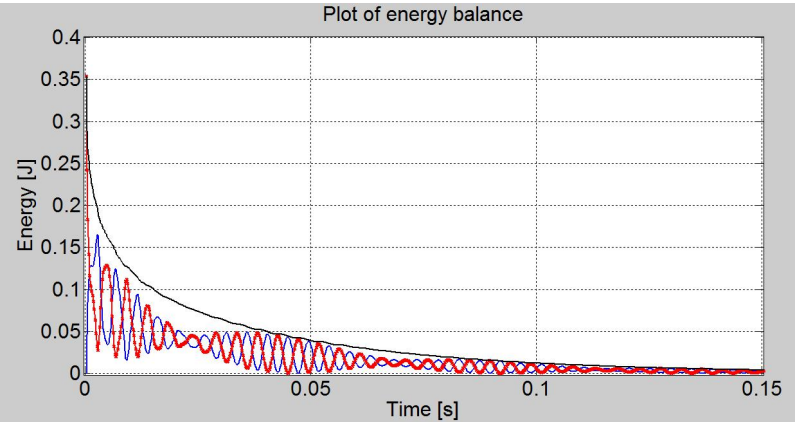

Figure 7: Graph of energy conservation for damping test. Potential energy E^s_{pot} is plotted with red crosses, kinetic energy E^s_{kin} blue and the total energy E^s is shown with black colour.

FSI test. For testing interaction between fluid and undamped elastic body, we prescribed to elastic body all initial and initial boundary conditions equal zero. The fluid setting was following: The kinematic viscosity was set $\nu^f = 1,5 \times 10^{-5}\,\mathrm{m/s^2}$ and the inlet boundary condition has a parabolic profile:

$$\mathbf{v}_{\mathrm{Dir}} = 0.025 \times \begin{pmatrix} 1913.26 \times (Y_i + 0.011)(0.017 - Y_i) \\ 0 \end{pmatrix}, \qquad [X_i, Y_i] \in \Gamma^f_{\mathrm{In}}. \tag{39}$$

The interaction was enabled after time $t = 0.1\,\mathrm{s}$, when the velocity profile behind the vocal fold was developed. The flow excited a periodic vibration of vocal fold with small amplitudes.

Figure 8 shows the approximation of the development of x-component velocity between time 0.05 and 0.3 s. The flow acceleration can be seen in Figure 8 in the narrowest part of the channel. Reynold's number for this setting was approximately 10.

Figure 9 and 10 show time signals of x-displacement and y-displacement of the point A in FSI test together with their Fourier transformation, respectively. The comparison with the modal analysis results demonstrates good agreement.

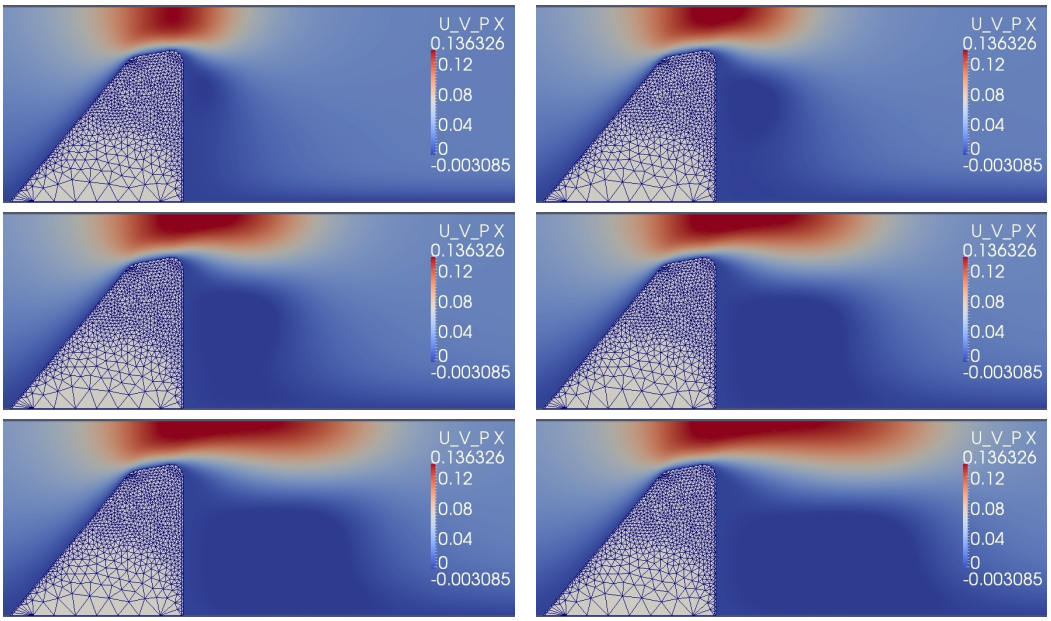

Figure 8: The flow x-velocity pattern around the fixed model at six different time instants $t = t_o + j \cdot 0.05\,\mathrm{s},\ (j = 0, \ldots, 5)$. Figures are ordered from the left to the right.

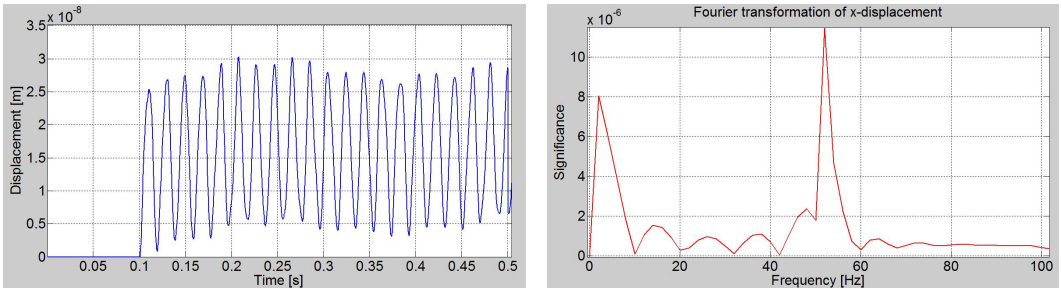

Figure 9: Time evolution of x-displacement of point A for the FSI test (left) and it's Fourier transformation with dominant frequency $f = 51\,\mathrm{Hz}$ (right).

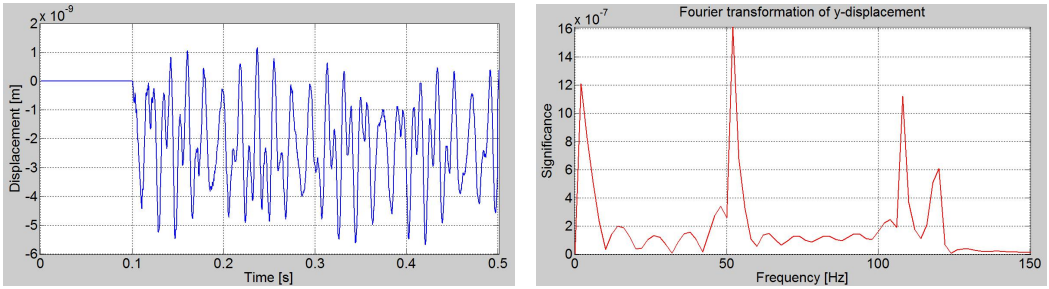

Figure 10: Time evolution of y-displacement of point A for the FSI test (left) and it's Fourier transformation with dominant frequency $f = 51\,\mathrm{Hz}$ (right).

5 Conclusion

The paper describes the formulation of the FSI problem demonstrated by the example of human fold vibration in airflow. The mathematical model is derived and then the numerical algorithm based on FEM and the ALE method is presented to simulate the behaviour of the coupled system. The developed numerical schemes were implemented in an own program, which is able to handle complex geometries. In the end the each part of the solver was tested by simply tests, which verifies it's basic functionality in the interaction problems.

Acknowledgment

The financial support for the present project was partly provided by the *Czech Science Foundation* under the *Grant No. 101/11/0207* and project *S*GS 13/174/OHK2/3T/12.

References

[1] Ascher, U. M.; Petzold, L. R.: Computer Methods for Ordinary Differential Equations and Differential-Algebraic Equations, *SIAM*, Philadelphia, 1998.

[2] Brdička, M., Samek, L., Sopko, B.:Mechanika kontinua. *Academia*, Praha, 2000. [in Czech]

[3] Curnier, A., Computational Methods in Solid Mechanics, *Kluwer Academic Publishing Group*, Dodrecht, 1994.

[4] Davis, T.: Umfpack. [mathematical library] Version 5.6.2. University of Florida, USA. Available at: http://www.cise.ufl.edu/research/sparse/umfpack/.

[5] Feistauer, M.: Mathematical Methods in Fluid Dynamics. *Logman Scientific & Technical*, Harlow, 1993.

[6] Feistauer, M. et al.: Numerical Simulation of Fluid-Structure Interaction Problems with Applications to Flow in Vocal Folds, *Fluid-Structure Interaction and Biomedical Applications*, edited by Bodnár, T., Galdi, G. P., Nečasová, S., Series: Advances in Mathematical Fluid Mechanics, XIV, pp. 312–393, Birkhauser, 2014. [Book chapter]

[7] Girault, V., Raviart, P., A.:Finite Element Methods for Navier-Stokes Equations. *Springer*, Berlin, 1986.

[8] Hadrava, M. & Feistauer M. & Horáček & Kosík, A.: Discontinuous Galerkin Method for the Problem of Linear Elasticity with Applications to the Fluid-Structure Interaction. *AIP Conference Proceedings*, vol. 1558, pp. 2348-2351; 2013.

[9] Kosík, A. & Feistauer, M. & Horáček , J. & Sváček, P.: Numerical Simulation of Interaction of Human Vocal Folds and Fluid Flow *Springer Proceedings in Physics*, vol. 139, pp. 765–771, 2011.

[10] Nomura, T. & Hughes, T. J. R.: An arbitrary Lagrangian-Eulerian finite element method for interaction of fluid and a rigid body. *Computer Methods in Applied Mechanics and Engineering*, vol. 95, pp. 115–138, 1992.

[11] Quarteroni, A. & Valli, A.: Numerical Approximation of Partial Differential Equations. *Springer*, Berlin, 1999.

[12] Scherer et al.: Intraglottal pressure profiles for a symmetric and oblique glottis with a divergence angle of 10 degrees *Journal Acoustic Society of America*, 4, 109, April 2001.

[13] Sváček, P. & Horáček , J.: Numerical Simulation of Glottal Flow in Interaction with Self Oscillating Vocal Folds: Comparison of Finite Element Approximation with a Simplified Model, *Communications in computational physics*, vol. 12, Issue: 3, pp. 789–806, 2012.

[14] Titze, I. R.: The Myoelastic Aerodynamic Theory of Phonation. National Center for Voice and Speech, USA, 2006.

[15] Valášek et al.: On Numerical Approximation of Fluid-Structure Interactions of Air Flow with a Model of Vocal Folds, *Topical problems of Fluid Mechanics 2015*, edited by D. Šimurda, T. Bodnár, pp. 245–254, 2015.